Atmospheric Research 153 (2015) 286–295

Contents lists available at ScienceDirect

Atmospheric Research

journal homepage: www.elsevier.com/locate/atmos

Characteristics of individual particles in the atmosphere of Guangzhou by single particle mass spectrometry

Guohua Zhang [a], Bingxue Han [a,b], Xinhui Bi [a,*], Shouhui Dai [a,b], Wei Huang [a,b], Duohong Chen [c], Xinming Wang [a], Guoying Sheng [a], Jiamo Fu [a], Zhen Zhou [d]

[a] State Key Laboratory of Organic Geochemistry, Guangzhou Institute of Geochemistry, Chinese Academy of Sciences, Guangzhou 510640, PR China
[b] Graduate University of Chinese Academy of Sciences, Beijing 100039, PR China
[c] State Environmental Protection Key Laboratory of Regional Air Quality Monitoring, Guangdong Environmental Monitoring Center, Guangzhou 510308, PR China
[d] Atmospheric Environment Institute of Safety and Pollution Control, Jinan University, Guangzhou 510632, PR China

ARTICLE INFO

Article history:
Received 26 May 2014
Received in revised form 25 July 2014
Accepted 28 August 2014
Available online 16 September 2014

Keywords:
Mixing state
Single particle
PRD
Single particle mass spectrometry
Secondary aerosol

ABSTRACT

Continuous ambient measurement of atmospheric aerosols was performed with a single particle aerosol mass spectrometer (SPAMS) in Guangzhou during summer of 2012. The aerosols mainly consisted of carbonaceous particles as major compositions in submicrometer range, including K-rich (29.8%), internally mixed organics and elemental carbon (ECOC, 13.5%), organic carbon-rich (OC, 18.5%), elemental carbon (EC, 12.3%) and high molecular OC (HMOC, 3.2%), and inorganic types (e.g., Na-rich Na-K, Fe-rich, V-rich, and Cu-rich) as major ones in supermicrometer range. Results show that carbonaceous particles were commonly internally mixed with sulfate and nitrate through atmospheric processing, in particular, with sulfate; inorganic types were dominantly internally mixed with nitrate rather than sulfate, indicative of different evolution processes for carbonaceous and inorganic particles in the atmosphere. It was observed that variations of these particle types were significantly influenced by air mass back trajectories (BTs). Under the influence of continental BTs, carbonaceous types were prevalent, while Na-K and Na-rich types considerably increased when the BTs originated from south marine regions. Number fraction of carbonaceous types exhibited obvious diurnal variation throughout the sampling period, which reflects their relatively stable emission and atmospheric processes. Two EC particle types LC-EC and NaK-EC showed different diurnal distributions, suggesting their different origins. The obtained information on the mixing state and the temporal variation of particle types is essential for developing an understanding on the origin and evolution processes of atmospheric aerosols.

© 2014 Elsevier B.V. All rights reserved.

1. Introduction

Atmospheric aerosols from anthropogenic and natural sources are the subject of enduring interest due to its effects on air quality, public health, and global climate change (Harrison and Yin, 2000; Pöschl, 2005; Watson, 2002). The impact of atmosphere aerosols on radiative forcing (Jacobson, 2001a,b; Kanakidou et al., 2005) and/or cloud condensation nuclei (CCN) (Sun and Ariya, 2006; Zhang et al., 2012) is highly dependent on their physical and chemical properties. Pearl River Delta (PRD) region faces increasing air pollution due to the rapid growing of population and the enhanced density of industrial activities (Chan and Yao, 2008). The air pollution problems have not only raised scientific interests, but also become a major concern of the government. Many measurements have shown that carbonaceous aerosols, sulfate and nitrate represent predominant fractions of fine particles, and significantly contribute to the regional haze formation in the PRD region (e.g., Andreae et al., 2008; Chan and Yao, 2008). Mixing state involving these compositions plays a substantially important role on the light extinction of ambient aerosols (Cheng et al., 2008; Yu

* Corresponding author. Tel.: +86 20 85290195; fax: +86 20 85290288.
E-mail address: bixh@gig.ac.cn (X. Bi).

http://dx.doi.org/10.1016/j.atmosres.2014.08.016
0169-8095/© 2014 Elsevier B.V. All rights reserved.

et al., 2010). However, mixing state of atmospheric aerosols, relying on single particle measurement, remains poorly understood in the PRD region, since previous measurements were primarily based on bulk aerosol filter samples that represent average chemical compositions (Chan and Yao, 2008; Tan et al., 2009; Tao et al., 2012).

To improve the understanding of the evolution of individual particles with distinctly different properties, it is essential to collect the physical and chemical information of atmospheric particles at single particle level with high time resolution (Prather, 2009; Pratt and Prather, 2012). The recent emergence and development of single particle mass spectrometry technology has been significantly advancing ambient individual particle characterization (Pratt et al., 2009; Su et al., 2004). It has been utilized to characterize size and mixing state of both ambient and laboratory generated aerosols, greatly improving the understanding on the aging processes, source, and optical properties of atmospheric aerosols (Moffet and Prather, 2009; Spencer et al., 2008; Sullivan et al., 2007). In China, on-line single particle mass spectrometry has most recently been applied in the studies on physicochemical properties of individual particles and their potential influence on air quality (Chen et al., 2014; Yang et al., 2012), and the related researches have investigated the mixing state of carbonaceous particles in the atmosphere of the PRD region (Bi et al., 2011; Zhang et al., 2013). However, knowledge on the mixing state of atmospheric aerosols in the PRD region was still limited.

The single particle studies have showed that there are many particle types with complex mixing state in the urban areas (e.g., Moffet et al., 2008a; Zhang et al., 2013). The physical and chemical properties (including density, shape, hygroscopicity, and refractive index) of these particle types are distinctly different from each other, influenced by various factors such as meteorological conditions and emission sources (e.g., Moffet and Prather, 2009; Zelenyuk et al., 2008). Therefore, it is expected that these particle types behave differently in the atmosphere and probably contribute differently to the environmental and climatic effect. In this study, a single particle aerosol mass spectrometer (SPAMS) was applied to characterize the physical and chemical properties of atmospheric aerosols with high time-resolution in Guangzhou, a megacity in the PRD region. We present three-week (1–21th August 2012) data on individual particles, including particle sizes and mass spectral characteristics. Located in a transitional zone of the East Asian monsoon system, Guangzhou experiences southwesterly summer monsoon, characterized by sea-land breezes during summer. High relative humidity (RH) and temperature (Temp) were frequently observed during this period. Coupled with meteorological conditions, the temporal profile, and size distribution of major particle types and also the influence of air mass on their mixing state were discussed.

2. Experiment set up

2.1. Sampling location and meteorological condition

Single particle measurements were carried out nearly continuously at Guangzhou Institute of Geochemistry (GIG), Chinese Academy of Sciences, during the summer (1–21th August) of 2012, using a SPAMS (Li et al., 2011) developed by Hexin Analytical Instrument Co., Ltd. (Guangzhou, China). Detail for the measurement site was described elsewhere (Bi et al., 2011). The sampling inlet was set up approximately 20 m above the ground level.

Temporal profiles (in 1 hour resolution) of local meteorological parameters, including solar radiation, Temp, RH, wind direction (WD) and wind speed (WS), and air quality parameters (i.e., NO_x, SO_2, O_3, PM_1) are shown in Fig. 1. Data for Temp, RH, WD, and WS was collected from Weather Underground (http://www.wunderground.com/), and the remaining parameters were provided by Guangdong Environmental Monitoring Center (http://www.gdemc.gov.cn/). The concentrations of NO_x, SO_2, and O_3 were measured by Model 42i ($NO–NO_2–NO_x$) Analyzer, Model 43i SO_2 Analyzer, and Model 49i O_3 Analyzer (Thermo Fisher Scientific Inc.), respectively. The concentrations of PM_1 and BC were continuously measured using a tapered element oscillating microbalance (TEOM 1405, Thermo Fisher Scientific Inc.) and a Multiangle Absorption Photometer (Model 5012, Thermo Fisher Scientific Inc.), respectively. Ambient Temp, RH, and WS during the field study varied between 23–38 °C, 37–100%, and 0–8 m/s, with average values of 30 °C, 77%, and 2 m/s, respectively. Temp, WS, and O_3 concentrations peaked at ~14:00 and reached their minimum at night, with RH showing an opposite trend. However, the concentration peaks for NO_x, SO_2, and PM_1 were often observed during the nighttime, due to the accumulation of pollutants under unfavorable meteorological conditions with lower WS and boundary layer depth.

2.1.1. Single particle acquisition and data analysis

Ambient aerosols were introduced from the sampling inlet to the SPAMS (Hexin Analytical Instrument Co., Ltd., Guangzhou, China), through a stainless steel tube (4 m). The particle detection method of SPAMS can be found elsewhere (Li et al., 2011). Briefly, particles are introduced into SPAMS through a critical orifice, then focused and accelerated to specific velocities that would be determined by two continuous diode Nd:YAG laser beams (532 nm) below in sizing region. Individual particle is then desorped/ionized by a pulsed laser (266 nm) triggered exactly based on the specific velocity. The positive and negative fragments generated are recorded with the recorded velocities. They were then converted to d_{va} using a calibration curve, created from the measured velocities of series of polystyrene latex spheres (Nanosphere Size Standards, Duke Scientific Corp., Palo Alto) with defined sizes.

Particle size and mass spectra information were imported into MATLAB (The MathWorks Inc.) and analyzed with YAADA (www.yaada.org), a MATLAB-based software toolkit for manipulating single particle mass spectral data set. We focus on the particles with vacuum aerodynamic diameter (d_{va}) ranging from 0.1 to 1.6 μm that were more effectively detected. The SPAMS collected approximately 750,000 individual particles with both positive and negative ion mass spectra. An adaptive resonance theory based neural network algorithm (ART-2a) is applied to cluster individual particles into separate groups based on the presence and intensity of ion peaks in single particle mass spectrum (Song et al., 1999), with a vigilance factor of 0.7, learning rate of 0.05, and 20 iterations. By merging similar clusters resulted from ART-2a, ten major particle types (16 if considering the subtypes) with distinct chemical patterns were obtained, representing ~92% of the population of the collected particles.

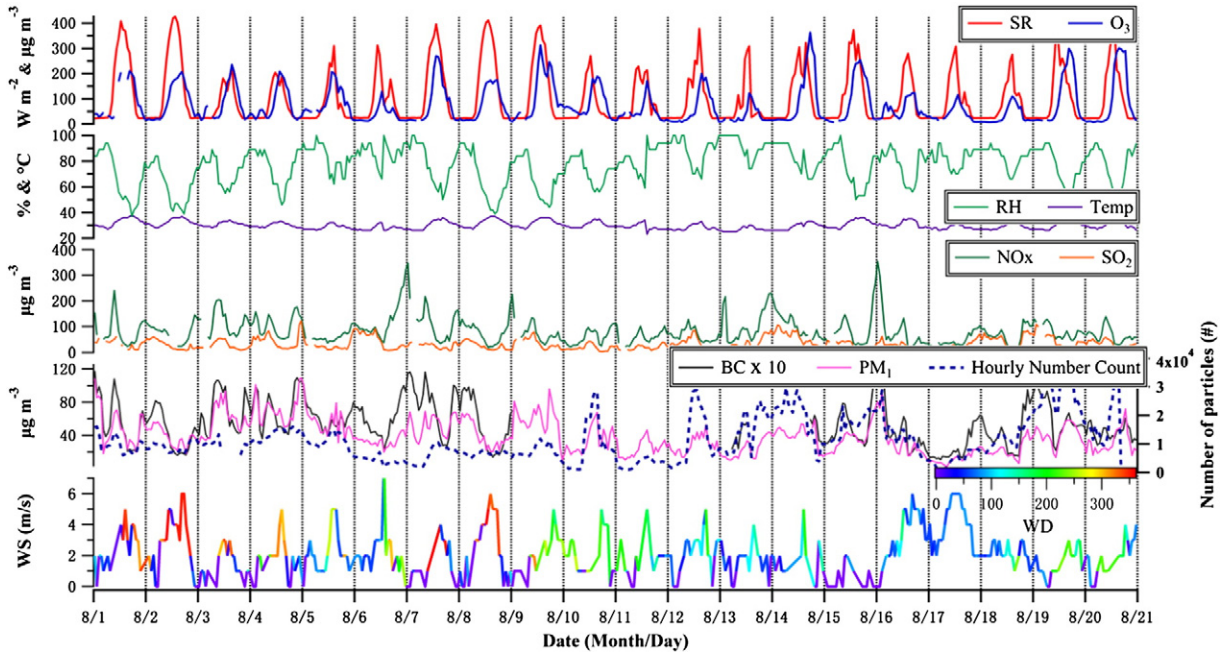

Fig. 1. Temporal profiles (in 1 h resolution) of PM_1 and black carbon (BC), gaseous pollutants (SO_2, NO_x, and O_3) and meteorological parameters, including temperature (Temp), relative humidity (RH), wind direction (WD), wind speed (WS), and solar radiation (SR), during the 1–21st of August 2012.

3. Results and discussion

The particle types with subtypes and their number fractions (Nf), relative to all the collected particles as mentioned above, are listed in Table 1. Carbonaceous particle types, including biomass/biofuel burning particles (K-rich, 29.8%), internally mixed organic and elemental carbon (ECOC, 13.5%), organic carbon-rich (OC, 15.3%), elemental carbon (EC, 12.3%), and high molecular OC (HMOC, 3.2%), dominated over the sampling period. The Nf of carbonaceous particles is comparable to that for spring and lower than that for fall in Guangzhou (Zhang et al., 2013). Inorganic types were dominated by Na-K (8.3%) and Na-rich (3.5%). The other 3 minor inorganic types were rich in transition metallic species, including Fe-rich, Cu-rich, and V-rich, accounting for 2.8%, 2.5%, and 0.9%, respectively. These metallic particle types are highlighted due to their potential health effects (Russell and Brunekreef, 2009). As discussed in Section 3.2, their Nf varied in a wide range and could reach as high as ~20–30% under specific meteorological condition.

Table 1
Summary of number count and fraction of the identified single particle classes in Guangzhou dataset.

Single particle classes	Number count	Nf[a]
K-rich	225,458	29.8%
Mainly with sulfate (K-S)	95,439	12.6%
With sulfate and nitrate (K-SN)	110,522	14.6%
Mainly with nitrate (K-N)	19,524	2.6%
ECOC	101,433	13.5%
Mainly with sulfate (ECOC-S)	95,732	12.7%
With sulfate and nitrate (ECOC-SN)	5701	0.8%
OC	115,960	18.5%
Mainly with sulfate (OC-S)	31,718	4.2%
With sulfate and nitrate (OC-SN)	81,735	10.8%
Mainly with nitrate (OC-N)	2507	0.3%
HMOC	24,562	3.2%
EC	93,125	12.3%
NaK-EC	68,604	9.1%
LC-EC	24,521	3.2%
Na-K	62,916	8.3%
Na-rich	26,274	3.5%
Fe-rich	21,413	2.8%
V-rich	6612	0.9%
Cu-rich	18,773	2.5%
Others[b]	59,568	7.9%

[a] Nf was calculated through dividing the number count of single particle classes by the total collected particle count.
[b] The remaining particles that were not clustered by ART-2a.

Particle types exhibited different size distributions depending upon their emissions and evolution mechanisms. Fig. 2 shows the Nf distribution of the particle types in a series of size bin (100 nm resolution). It can be seen that the Nf for each particle type is highly dependent on d_{va}. Significant divergence in chemical compositions is found between submicrometer (0.1–1.0 μm) and supermicrometer (1.0–1.6 μm) particles. Carbonaceous types concentrated in submicrometer particles, while supermicrometer particles were dominated by inorganic types. EC types (NaK-EC and LC-EC) showed similar distribution that the Nf decreased with increasing d_{va}, and represented the highest fraction (41–67%) in the size range of 0.1–0.3 μm. K-rich types dominated (31–39%) in the size range of 0.3–0.8 μm. The highest fractions for ECOC (~20%) and OC (29–35%) were found in the size range of 0.5–0.7 and 0.3–0.5 μm, respectively. Na-rich represented a dominant fraction (21–41%) in the supermicrometer particles, followed by Na-K (13–16%). This distribution pattern is similar to those reported for a coastal city in the USA (Qin et al., 2012).

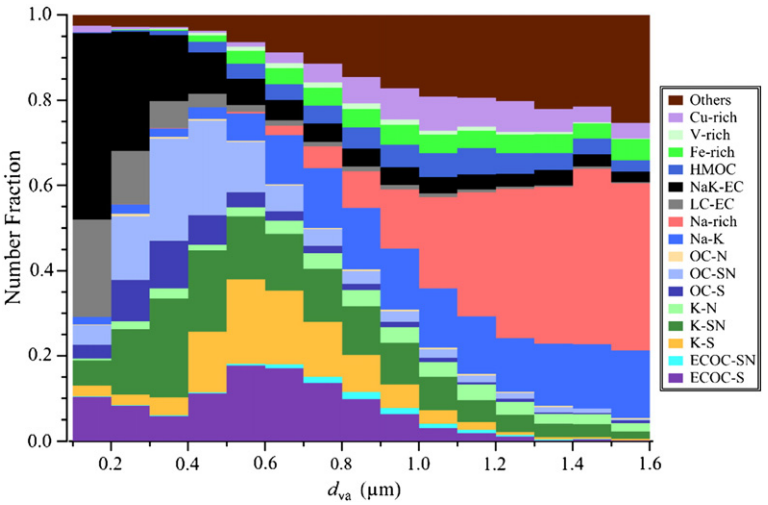

Fig. 2. Size-resolved Nf distribution of the particle types (in 100 nm resolution) throughout the sampling period.

3.1. Mass spectral and mixing state characteristics of the particle types

Representative mass spectra for the particle types are displayed in Fig. 3. Each particle type is labeled according to the most significant chemical features in the mass spectra, and the corresponding characteristics are briefly described as follows.

Carbonaceous types: The K-rich particles contain potassium ($39[K]^+$), sulfate ($-97[HSO_4]^-$), nitrate ($-46[NO_2]^-$ and -62 $[NO_3]^-$), and carbonaceous species (e.g., $12[C]^+$, $27[C_2H_3]^+$, 29 $[C_2H_5]^+$, $36[C_3]^+$, $37[C_3H]^+$, $43[C_2H_3O]^+$, $-26[CN]^-$, -42 $[CNO]^-$) as major components, similar to those reported in other studies (Moffet et al., 2008a; Silva et al., 1999). The association of sulfate and nitrate indicates that K-rich particles experienced atmospheric aging. It was reported that potassium chloride (KCl) occurs in young smoke of biomass burning, whereas amounts of K_2SO_4 and KNO_3 increased as the smoke aging, due to rapid substitution of chloride by sulfate and nitrate during the transport (Zauscher et al., 2013). ECOC particles have typical carbon ion clusters ($12[C]^{+/-}$, $24[C_2]^{+/-}$,..., $12n[C_n]^{+/-}$) with $36[C_3]^+$ as dominant fragments, together with OC markers (e.g., $27[C_2H_3]^+$, $29[C_2H_5]^+$, $37[C_3H]^+$, and $43[C_2H_3O]^+$). Mass spectra for OC particles mainly contain the OC markers, and also some other OC peaks such as $50[C_4H_2]^+$, $51[C_4H_3]^+$, $55[C_4H_7]^+$ and $63[C_5H_3]^+$. Besides, a large peak at m/z 39 is also observed in mass spectra of OC, which might be explained by coagulation between OC and $39[K]^+$ or condensation of organic species onto biomass seed (Moffet et al., 2008a). Particle mass spectra in HMOC type show the presence of m/z 50, 51, 63, 77, 91, 115, and 128 (Silva and Prather, 2000; Sodeman et al., 2005). Mass spectra of LC-EC type are dominated by the distinct carbon ion clusters ranged from m/z −120 to m/z 180, with minor ion intensities from other species. Differently, NaK-EC type shows the carbon ion clusters mainly in the negative mass spectra, combined with dominant peaks from $23[Na]^+$ and $39[K]^+$ in the positive ones.

Inorganic particle types: Na-K type is characterized by dominant peaks from $39[K]^+$, relatively less intense peak from $23[Na]^+$, nitrate and silicate ($-76[SiO_3]^-$). They are probably from dust and/or industry sources, as indicated by the presence of silicate (Moffet et al., 2008a), and also their size distribution. Peaks corresponding to $23[Na]^+$, $39[K]^+$, $46[Na_2]^+$, 81/83 $[Na_2Cl]^+$, nitrate and chloride ($-35[Cl]^-$ and $-37[Cl]^-$) are present in mass spectra of Na-rich, indicating transport and evolution of sea salt particles (Gaston et al., 2011, 2013). The presence of nitrate in Na-rich particles implies the replacement of chloride by nitrate during long-range transport (Gard et al., 1998; Zhao and Gao, 2008). Fe-rich type is identified by strong peaks from iron at m/z 54, 56 and 57, according to their isotopic components. Fe-rich particles could be emitted through metallic industry, coal combustion, and biomass burning (Chen et al., 2012; Guieu et al., 2005). Particle type V-rich is identified according to the strong signals due to vanadium ($51[V]^+$ and $67[VO]^+$), mainly attributed to emission from ship traffic (Ault et al., 2010; Zhao et al., 2013), and also to vehicle exhausts in minor fraction (Shields et al., 2007; Sodeman et al., 2005). Cu-rich is characterized by the presence of isotopic peaks at m/z 63 and 65, commonly associated with Na, K, Fe, Pb, chloride, nitrate, and sulfate. In addition, inorganic types contained negligible signals from carbonaceous species, indicative of their externally mixing state. Externally mixing of carbon with particles containing chloride and nitrate salts of metals such as Pb and Zn has been observed in the urban atmosphere and these types were attributed to industrial waste incineration (Moffet et al., 2008b). As presented above and discussed in Section 3.2, carbonaceous and inorganic particle types showed totally different size distribution patterns and thus it is expected that they originated from different sources.

Secondary inorganic species like sulfate, nitrate and ammonium were commonly detected in different single particle types with different intensities (Cahill et al., 2012; Zhang et al., 2013). The presence of secondary species on the particle types provides an indication of chemical processes in the atmosphere (Spencer et al., 2008). Several secondary markers (i.e., m/z 18, −46, −62 and −97) and other markers (m/z −35/−37 for chloride, and m/z 36 for carbon) are selected to show their association with each particle types. Note that sulfate, nitrate, ammonium, and carbonaceous compositions represent dominant fractions of submicrometer particles, while chloride contributes limit fraction in the atmosphere of the PRD region (He et al., 2011; Huang et al., 2011). Fig. 4 displays the Nf of several markers on each

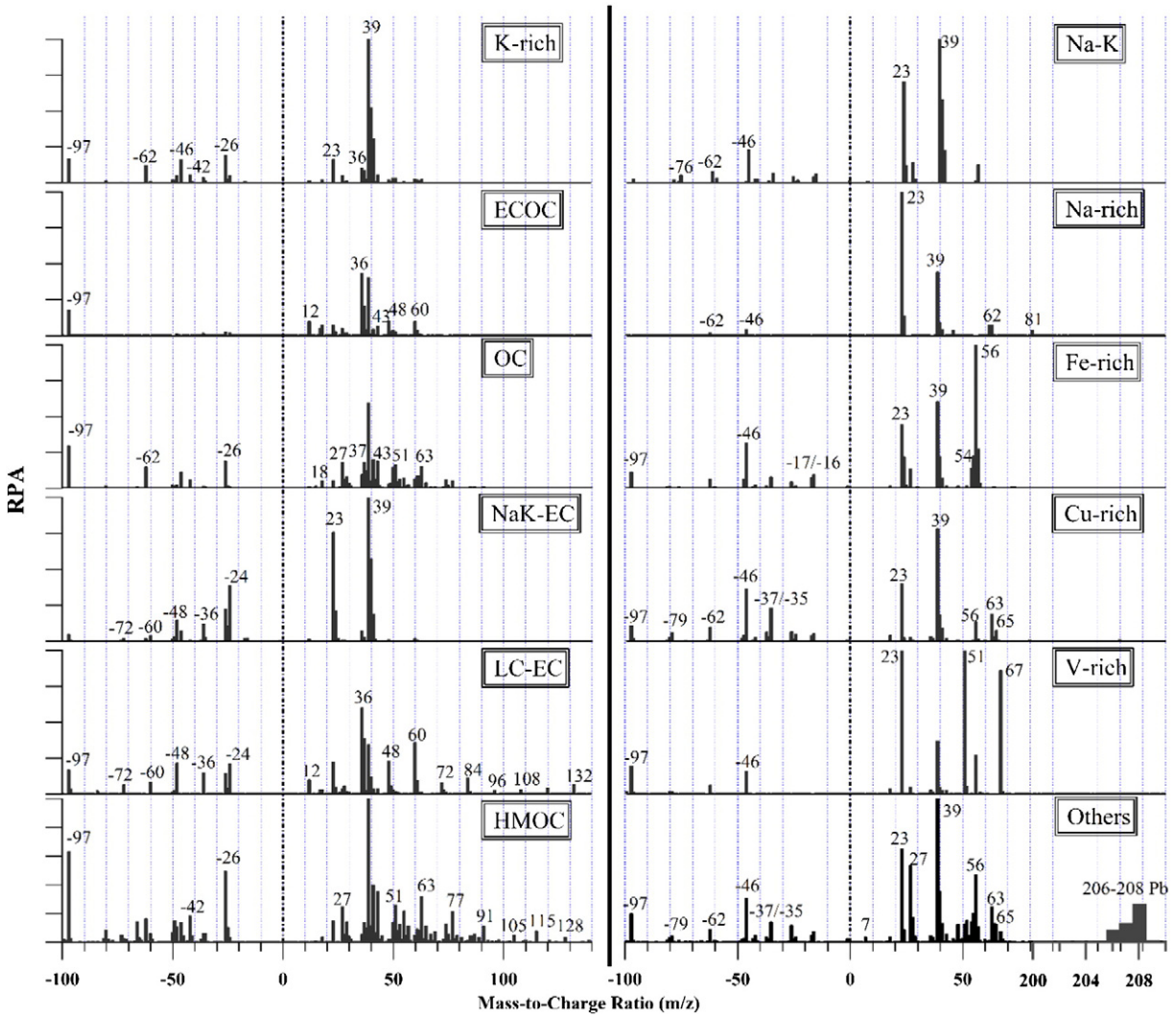

Fig. 3. Average mass spectra for particle types identified in the atmosphere of the PRD region during summer of 2012. "Others" represented the remaining particles that were not classified. Their mass spectral characteristics indicate that they were similar to inorganic types, containing many metallic species, such as Pb, Cu, and Fe.

particle types. Most carbonaceous types associated with more sulfate than nitrate, which should be attributed to the chemical composition patterns in the atmosphere of the PRD region, and also due to different formation mechanisms of sulfate and nitrate (Seinfeld and Pandis, 2006; Xiao et al., 2009). Carbonaceous types, except K-N and OC-N, associated with much more sulfate than inorganic types. More than 90% of carbonaceous particles contained detectable amount of sulfate, while the Nf of inorganic

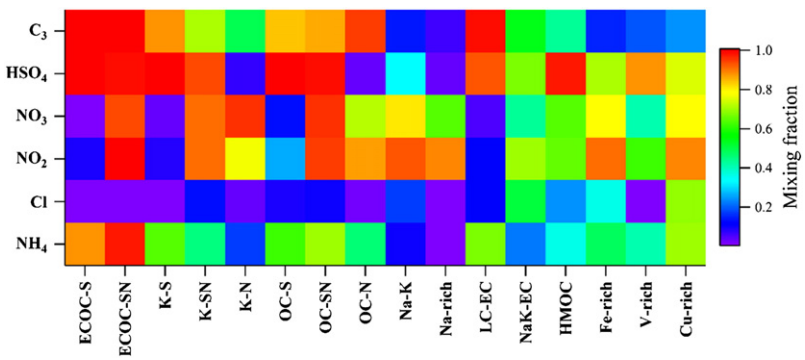

Fig. 4. Nf of several selected markers associated with the particle types, indicated by the coloration.

types that associated with sulfate is generally less than 80%. Exception is found for V-rich particles which were extensively internally mixed with sulfate, probably due to promotion of sulfate formation catalyzed by V (Ault et al., 2010). The Nf of sulfate is lower (i.e., <40%) for Na-rich and Na-K types; however, that of nitrate (>80%) is relatively high, indicating different evolution mechanisms of these particles compared to carbonaceous types. The distribution of ammonium is generally consistent with that of sulfate, with higher fraction in carbonaceous types, due to the strong association of ammonium and sulfate (Seinfeld and Pandis, 2006). Chlorine was mainly associated with inorganic types, mostly in Cu-rich, indicative of primary emission of $CuCl_2$. The strong association of Cu-rich with sulfate and nitrate suggests that $CuCl_2$ underwent heterogeneous displacement reactions with HNO_3 and H_2SO_4 (Moffet et al., 2008a).

3.2. Influences of back trajectory on the distribution of the particle types

To explore the influence of pollutant transport on PM_1 loading and particle type patterns in Guangzhou, back trajectory (BT) analysis, with HYSPLIT 4.9 transport model (http://ready.arl.noaa.gov/HYSPLIT.php) (Draxler and Rolph, 2012), was performed. Seventy-two-hour air mass back trajectories simulated every 12 h, ending at 200 m above the ground level of the site, are shown in Fig. S1 of Supplementary data. The BTs mainly consisted of four groups, including air masses from southern marine (SM, 53.5%), northeastern continent (NC, 22.5%), northeastern continent regional areas (NCRA, 11.5%), and western continent regional areas (WCRA, 10%). The mean PM_1, gaseous pollutants, and meteorological parameters corresponding to the different BTs are listed in Table 2. During the 1–9th of August, continental BTs (i.e., NC, NCRA, and WCRA) dominated with high PM_1 mass concentration of 48.8–59.1 μg m^{-3}, representing polluted air mass origin. The NC and NCRA BTs were associated with high fraction (38.4% and 52.6%, respectively) of calm period (when WS <1 m/s) (Fig. S2), causing effective pollutant accumulation. The air masses shifted to SM regions during the 10–20th of August, which represented the clean air mass with mean PM_1 of ~30 μg m^{-3}. The BT analysis highlights that regional transport from the continent is the most unfavorable meteorological condition for submicrometer aerosol pollution in Guangzhou.

Fig. 5 displays the temporal variation of the Nf of the particle types, and their distribution grouped by BT types. Regardless of the variation of the BTs, carbonaceous types, such as K-rich and ECOC, showed a regular variation throughout the whole sampling period, indicating that there are some stable local and/or regional sources, such as biomass/biofuel burning, industries and vehicles (Cao et al., 2004; Hagler et al., 2006). However, the inorganic types varied considerably without a regular trend. Under the influence of continental BTs during the 1–9th of August, carbonaceous types were more prevalent (78–85%), while Na-K and Na-rich types were limited and/or negligible. Fractional distribution of carbonaceous types is also similar for NCRA, NC, and WCRA BTs. During the 10–20th of August, inorganic types increased considerably (from ~8% to ~22%), in particular Na-K and Na-rich types, under the influence of SM BTs. The highest Nf of Na-K and Na-rich types were ~32% and ~38%, respectively. Notably, during the 17–18th of August, Nf of inorganic types was comparable to that of carbonaceous particles, indicating a strong influence of SM BTs on the air quality of Guangzhou. Fe-rich, V-rich, and Cu-rich types also peaked under the influence of SM BTs. Major Fe-rich peaks with $Nf_{Fe\text{-}rich}$ up to ~14% were observed during the 12–15th of August. Major peaks for Cu-rich occurred during nighttime (02:00–07:00 and 20:00–08:00 on 18–19th of August), with $Nf_{Cu\text{-}rich}$ at ~17% and ~23%, respectively. While Na-rich particles were generated by the spray of sea water, Na-K, Fe-rich, V-rich, and Cu-rich particle types were more probably brought in as the BTs passed through the continental areas, from local and/or regional sources. The different distribution patterns for particle types under the influence of SM and other BTs should be attributed to the different emission patterns of the southern areas around Guangzhou, with more contribution from industries (Cheng et al., 2013). The difference can also be reflected by higher amount of SO_2 and lower amount of NO_x and BC (Table 2) associated with the SM BTs. In addition, the fractional size distribution was relatively stable for submicrometer particles throughout the study, dominated by carbonaceous types, and was variable for the supermicrometer particles, through the invasion of the inorganic particles, in particular, under the influence of SM BTs (Fig. S3).

Table 2
Summary of meteorological parameters and corresponding Nf of the 11 particle types associated with different BTs.

	NCRA (11.5% [a])	NC (22.5%)	WCRA (10%)	SM (53.5%)
WS (m/s)	0.9	1.7	2.0	1.9
T (°C)	30.6	31.7	30.6	28.8
RH%	78.4	68.8	71.3	82.3
Vis (Km)	9.9	12.3	9.2	11.7
PM_1 [b]	49.8	48.8	59.1	30.0
$PM_{2.5}$	60.3	60.1	77.2	38.3
NO*x*	124	92.7	75.1	73.8
SO_2	27.9	29.8	33.2	36.1
BC	7.8	5.6	7.3	4.5
Carbonaceous%	78%	85%	83%	70%
Inorganic%	13%	8%	9%	22%

[a] The Nf of the BTs during the 1–21th of August 2012.
[b] The unit for PM_1, $PM_{2.5}$, NO*x*, SO_2, and BC is μg m^{-3}.

3.3. Diurnal patterns for the particle types

The averaged diurnal variations for the particle types are displayed in Fig. 6, which shows that Nf of the particle types varied in a wide range. Most carbonaceous types showed pronounced diurnal patterns. Diurnal variation of $Nf_{ECOC\text{-}S}$ (2–38%) and $Nf_{K\text{-}S}$ (1–33%) showed nearly identical pattern with a major peak in the afternoon (13:00–15:00). $Nf_{ECOC\text{-}SN}$, $Nf_{K\text{-}N}$, and $Nf_{K\text{-}SN}$ showed opposite distributions with the highest value at the night. These diurnal patterns suggest that ECOC-S and K-S shared similar physicochemical processes in the atmosphere, and that mixing state of ECOC and K-rich particles with sulfate and nitrate were highly variable. The highly internal mixing state with sulfate for ECOC and K-rich types in the afternoon is attributed to active formation of sulfate from photochemical oxidation of SO_2 in the PRD region (Xiao et al., 2009), and the evaporative nature of nitrate

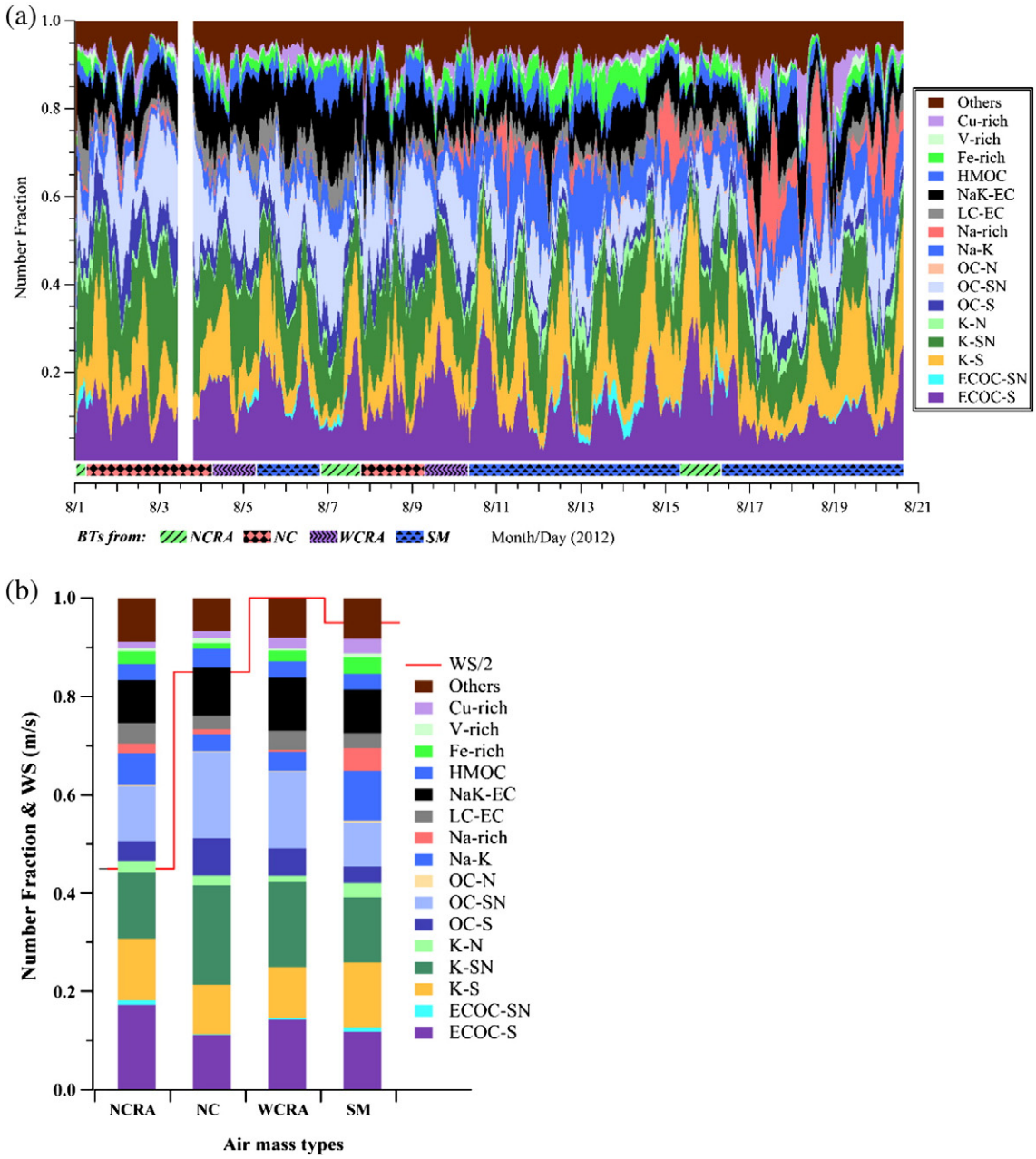

Fig. 5. (a) Temporal profiles of Nf of the particle types (in 1 h resolution), coupled with marked BTs at the bottom, and (b) Nf of the particle types (bar plot) and average WS (red line) associated with four type of BTs, i.e., NCRA, NC, WCRA, and SM BTs, respectively.

(Seinfeld and Pandis, 2006). The results also imply that nitrate condensed onto the ECOC-S and K-S to form ECOC-SN and K-SN during the nighttime with lower T and higher RH. The diurnal trends for $Nf_{OC\text{-}SN}$, $Nf_{OC\text{-}N}$, and Nf_{HMOC} are similar to that for $Nf_{K\text{-}SN}$ and the mass spectra for these particle types commonly had intense $39[K]^+$ signals, indicative of their similar origins, i.e., biomass burning. LC-EC showed a major peak in the afternoon (15:00–16:00) and a minor peak in the morning (6:00–7:00), while NaK-EC singly peaked in the early morning (4:00–6:00), with the lowest fraction in the afternoon (15:00–16:00). The distinctly different mixing state and temporal distributions between two EC types suggest their different origins. Therefore, EC types should be clustered more carefully in single particle studies. They may also have different optical properties, as indicated from their light scattering signals recorded by SPAMS during particle sizing (data no shown). The optical properties of these particle types will be explored in future studies. Generally, the variations of inorganic types were associated with large uncertainty, showing no regular variation, attributed to the strong influence of air mass types. However, it can still be seen that Na-rich and Fe-rich particles were more abundant during daytime.

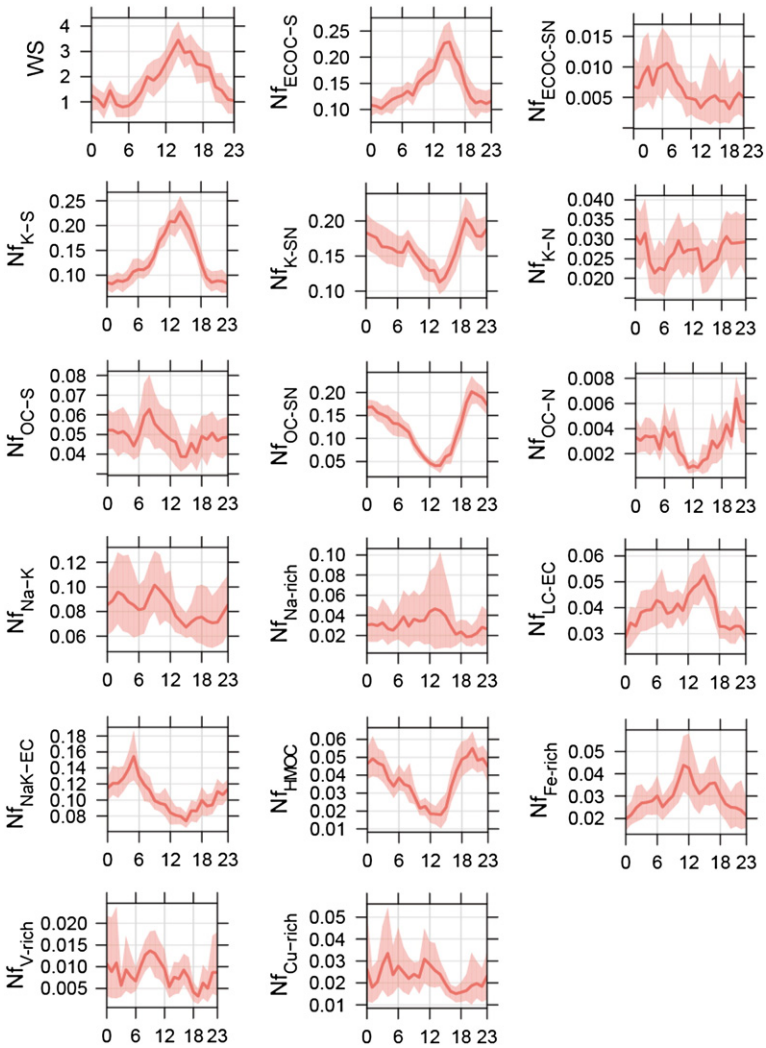

Fig. 6. Average diurnal patterns of Nf of the particle types and WS. The covered coloration indicates the standard deviation.

4. Conclusions

This paper provides detail size, mass spectral and temporal characteristics of the individual particles in the atmosphere of Guangzhou, during the summer of 2012. Analysis of the mass spectra revealed several particle clusters, including ECOC, K-rich, OC, EC, HMOC, and Na-K, Na-rich, Fe-rich, V-rich, and Cu-rich, assigned to both natural and anthropogenic-sources from continental and marine regions. Overall, carbonaceous types consist of K-rich and ECOC as major fraction types dominated in the submicrometer size range. In contrast, the supermicrometer range was dominated by inorganic Na-rich and Na-K types. Transition metals (Fe, V, and Cu) were also mostly detected in this size range. Carbonaceous types were internally mixed with more sulfate, while inorganic types with more nitrate. Active photochemical processes in the afternoon increased the fraction of internally mixed K-rich and ECOC particles with sulfate. Aerosol properties varied considerably, strongly influenced by air mass histories. Urban and industrial emissions advected from continental regions resulted in higher particulate mass and carbonaceous compositions. Cleaner air from southern marine and coastal regions carried aerosols with relatively higher fractions of inorganic types. Most carbonaceous types showed pronounced diurnal patterns and two EC particle types showed different diurnal pattern. LC-EC showed a major peak in the afternoon and a minor peak in the morning while NaK-EC only peaked in the early morning. The analysis has revealed physical and chemical properties of various particle types in the atmosphere of Guangzhou and their influence factors, which should be considered in predictions of their impacts on the environment.

Acknowledgement

This work was supported by the “Strategic Priority Research Program (B)” of the Chinese Academy of Sciences (XDB05020205), "The Team Project for Natural Science Foundation of Guangdong Province, China" (S2012030006604) and State Key Laboratory of Organic Geochemistry (SKLOG2013A01). G.H. Zhang thanks support from China Postdoctoral Science

Foundation Funded Project (2014M550442). The authors also gratefully acknowledge the NOAA Air Resources Laboratory (ARL) for the provision of the HYSPLIT transport and dispersion model and/or READY website (http://ready.arl.noaa.gov) used in this publication. This is contribution from CASGIG NO.1954.

Appendix A. Supplementary data

Supplementary data to this article can be found online at http://dx.doi.org/10.1016/j.atmosres.2014.08.016.

References

Andreae, M.O., Schmid, O., Yang, H., Chand, D.L., Yu, J.Z., Zeng, L.M., Zhang, Y.H., 2008. Optical properties and chemical composition of the atmospheric aerosol in urban Guangzhou, China. Atmos. Environ. 42, 6335–6350.

Ault, A.P., Gaston, C.J., Wang, Y., Dominguez, G., Thiemens, M.H., Prather, K.A., 2010. Characterization of the single particle mixing state of individual ship plume events measured at the port of Los Angeles. Environ. Sci. Technol. 44, 1954–1961.

Bi, X.H., Zhang, G.H., Li, L., Wang, X.M., Li, M., Sheng, G.Y., Fu, J.M., Zhou, Z., 2011. Mixing state of biomass burning particles by single particle aerosol mass spectrometer in the urban area of PRD, China. Atmos. Environ. 45, 3447–3453.

Cahill, J.F., Suski, K., Seinfeld, J.H., Zaveri, R.A., Prather, K.A., 2012. The mixing state of carbonaceous aerosol particles in northern and southern California measured during CARES and CalNex 2010. Atmos. Chem. Phys. 12, 10989–11002.

Cao, J.J., Lee, S.C., Ho, K.F., Zou, S.C., Fung, K., Li, Y., Watson, J.G., Chow, J.C., 2004. Spatial and seasonal variations of atmospheric organic carbon and elemental carbon in Pearl River Delta Region, China. Atmos. Environ. 38, 4447–4456.

Chan, C.K., Yao, X., 2008. Air pollution in mega cities in China. Atmos. Environ. 42, 1–42.

Chen, H., Laskin, A., Baltrusaitis, J., Gorski, C.A., Scherer, M.M., Grassian, V.H., 2012. Coal fly ash as a source of iron in atmospheric dust. Environ. Sci. Technol. 46, 2112–2120.

Chen, K., Yin, Y., Kong, S.F., Xiao, H., Wu, Y.X., Chen, J.H., Li, A.H., 2014. Size-resolved chemical composition of atmospheric particles during a straw burning period at Mt. Huang (the Yellow Mountain) of China. Atmos. Environ. 84, 380–389.

Cheng, Y.F., Wiedensohler, A., Eichler, H., Su, H., Gnauk, T., Brüggemann, E., Herrmann, H., Heintzenberg, J., Slanina, J., Tuch, T., Hu, M., Zhang, Y.H., 2008. Aerosol optical properties and related chemical apportionment at Xinken in Pearl River Delta of China. Atmos. Environ. 42, 6351–6372.

Cheng, S.Y., Wang, F., Li, J.B., Chen, D.S., Li, M.J., Zhou, Y., Ren, Z.H., 2013. Application of trajectory clustering and source apportionment methods for investigating trans-boundary atmospheric PM10 pollution. Aerosol Air Qual. Res. 13, 333–342.

Draxler, R.R., Rolph, G.D., 2012. HYSPLIT (HYbrid Single-Particle Lagrangian Integrated Trajectory) Model access via NOAA ARL READY Website. http://ready.arl.noaa.gov/HYSPLIT.php (MD, Silver Spring).

Gard, E.E., Kleeman, M.J., Gross, D.S., Hughes, L.S., Allen, J.O., Morrical, B.D., Fergenson, D.P., Dienes, T., Galli, M.E., Johnson, R.J., Cass, G.R., Prather, K.A., 1998. Direct observation of heterogeneous chemistry in the atmosphere. Science 279, 1184–1187.

Gaston, C.J., Furutani, H., Guazzotti, S.A., Coffee, K.R., Bates, T.S., Quinn, P.K., Aluwihare, L.I., Mitchell, B.G., Prather, K.A., 2011. Unique ocean-derived particles serve as a proxy for changes in ocean chemistry. J. Geophys. Res. Atmos. 116, 1–13.

Gaston, C.J., Quinn, P.K., Bates, T.S., Gilman, J.B., Bon, D.M., Kuster, W.C., Prather, K.A., 2013. The impact of shipping, agricultural, and urban emissions on single particle chemistry observed aboard the R/V Atlantis during CalNex. J. Geophys. Res. Atmos. 118, 5003–5017.

Guieu, C., Bonnet, S., Wagener, T., Loye-Pilot, M.D., 2005. Biomass burning as a source of dissolved iron to the open ocean? Geophys. Res. Lett. 32, 1–5.

Hagler, G.S., Bergin, M.H., Salmon, L.G., Yu, J.Z., Wan, E.C.H., Zheng, M., Zeng, L.M., Kiang, C.S., Zhang, Y.H., Lau, A.K.H., Schauer, J.J., 2006. Source areas and chemical composition of fine particulate matter in the Pearl River Delta region of China. Atmos. Environ. 40, 3802–3815.

Harrison, R.M., Yin, J.X., 2000. Particulate matter in the atmosphere: which particle properties are important for its effects on health? Sci. Total Environ. 249, 85–101.

He, L.Y., Huang, X.F., Xue, L., Hu, M., Lin, Y., Zheng, J., Zhang, R.Y., Zhang, Y.H., 2011. Submicron aerosol analysis and organic source apportionment in an urban atmosphere in Pearl River Delta of China using high-resolution aerosol mass spectrometry. J. Geophys. Res. Atmos. 116, 1–15.

Huang, X.F., He, L.Y., Hu, M., Canagaratna, M.R., Kroll, J.H., Ng, N.L., Zhang, Y.H., Lin, Y., Xue, L., Sun, T.L., Liu, X.G., Shao, M., Jayne, J.T., Worsnop, D.R., 2011. Characterization of submicron aerosols at a rural site in Pearl River Delta of China using an Aerodyne High-Resolution Aerosol Mass Spectrometer. Atmos. Chem. Phys. 11, 1865–1877.

Jacobson, M.Z., 2001a. Global direct radiative forcing due to multicomponent anthropogenic and natural aerosols. J. Geophys. Res. Atmos. 106, 1551–1568.

Jacobson, M.Z., 2001b. Strong radiative heating due to the mixing state of black carbon in atmospheric aerosols. Nature 409, 695–697.

Kanakidou, M., Seinfeld, J.H., Pandis, S.N., Barnes, I., Dentener, F.J., Facchini, M.C., Van Dingenen, R., Ervens, B., Nenes, A., Nielsen, C.J., Swietlicki, E., Putaud, J.P., Balkanski, Y., Fuzzi, S., Horth, J., Moortgat, G.K., Winterhalter, R., Myhre, C.E.L., Tsigaridis, K., Vignati, E., Stephanou, E.G., Wilson, J., 2005. Organic aerosol and global climate modelling: a review. Atmos. Chem. Phys. 5, 1053–1123.

Li, L., Huang, Z.X., Dong, J.G., Li, M., Gao, W., Nian, H.Q., Fu, Z., Zhang, G.H., Bi, X.H., Cheng, P., Zhou, Z., 2011. Real time bipolar time-of-flight mass spectrometer for analyzing single aerosol particles. Int. J. Mass Spectrom. 303, 118–124.

Moffet, R.C., Prather, K.A., 2009. In-situ measurements of the mixing state and optical properties of soot with implications for radiative forcing estimates. Proc. Natl. Acad. Sci. U. S. A. 106, 11872–11877.

Moffet, R.C., de Foy, B., Molina, L.T., Molina, M.J., Prather, K.A., 2008a. Measurement of ambient aerosols in northern Mexico City by single particle mass spectrometry. Atmos. Chem. Phys. 8, 4499–4516.

Moffet, R.C., Desyaterik, Y., Hopkins, R.J., Tivanski, A.V., Gilles, M.K., Wang, Y., Shutthanandan, V., Molina, L.T., Abraham, R.G., Johnson, K.S., Mugica, V., Molina, M.J., Laskin, A., Prather, K.A., 2008b. Characterization of aerosols containing Zn, Pb, and Cl from an industrial region of Mexico City. Environ. Sci. Technol. 42, 7091–7097.

Pöschl, U., 2005. Atmospheric aerosols: composition, transformation, climate and health effects. Angew. Chem. Int. Ed. 44, 7520–7540.

Prather, K.A., 2009. Our current understanding of the impact of aerosols on climate change. ChemSusChem 2, 377–379.

Pratt, K.A., Prather, K.A., 2012. Mass spectrometry of atmospheric aerosols—recent developments and applications. Part II: on-line mass spectrometry techniques. Mass Spectrom. Rev. 31, 17–48.

Pratt, K.A., Mayer, J.E., Holecek, J.C., Moffet, R.C., Sanchez, R.O., Rebotier, T.P., Furutani, H., Gonin, M., Fuhrer, K., Su, Y.X., Guazzotti, S., Prather, K.A., 2009. Development and characterization of an aircraft aerosol time-of-flight mass spectrometer. Anal. Chem. 81, 1792–1800.

Qin, X.Y., Pratt, K.A., Shields, L.G., Toner, S.M., Prather, K.A., 2012. Seasonal comparisons of single-particle chemical mixing state in Riverside, CA. Atmos. Environ. 59, 587–596.

Russell, A.G., Brunekreef, B., 2009. A focus on particulate matter and health. Environ. Sci. Technol. 43, 4620–4625.

Seinfeld, J.H., Pandis, S.N., 2006. Atmospheric Chemistry and Physics: From Air Pollution to Climate Change, New Jersey.

Shields, L.G., Suess, D.T., Prather, K.A., 2007. Determination of single particle mass spectral signatures from heavy-duty diesel vehicle emissions for PM2.5 source apportionment. Atmos. Environ. 41, 3841–3852.

Silva, P.J., Prather, K.A., 2000. Interpretation of mass spectra from organic compounds in aerosol time-of-flight mass spectrometry. Anal. Chem. 72, 3553–3562.

Silva, P.J., Liu, D.Y., Noble, C.A., Prather, K.A., 1999. Size and chemical characterization of individual particles resulting from biomass burning of local Southern California species. Environ. Sci. Technol. 33, 3068–3076.

Sodeman, D.A., Toner, S.M., Prather, K.A., 2005. Determination of single particle mass spectral signatures from light-duty vehicle emissions. Environ. Sci. Technol. 39, 4569–4580.

Song, X.H., Hopke, P.K., Fergenson, D.P., Prather, K.A., 1999. Classification of single particles analyzed by ATOFMS using an artificial neural network, ART-2A. Anal. Chem. 71, 860–865.

Spencer, M.T., Holecek, J.C., Corrigan, C.E., Ramanathan, V., Prather, K.A., 2008. Size-resolved chemical composition of aerosol particles during a monsoonal transition period over the Indian Ocean. J. Geophys. Res. Atmos. 113, 1–14.

Su, Y.X., Sipin, M.F., Furutani, H., Prather, K.A., 2004. Development and characterization of an aerosol time-of-flight mass spectrometer with increased detection efficiency. Anal. Chem. 76, 712–719.

Sullivan, R.C., Guazzotti, S.A., Sodeman, D.A., Prather, K.A., 2007. Direct observations of the atmospheric processing of Asian mineral dust. Atmos. Chem. Phys. 7, 1213–1236.

Sun, J., Ariya, P., 2006. Atmospheric organic and bio-aerosols as cloud condensation nuclei (CCN): a review. Atmos. Environ. 40, 795–820.

Tan, J.H., Duan, J.C., Chen, D.H., Wang, X.H., Guo, S.J., Bi, X.H., Sheng, G.Y., He, K.B., Fu, J.M., 2009. Chemical characteristics of haze during summer and winter in Guangzhou. Atmos. Res. 94, 238–245.

Tao, J., Shen, Z.X., Zhu, C.S., Yue, J.H., Cao, J.J., Liu, S.X., Zhu, L.H., Zhang, R.J., 2012. Seasonal variations and chemical characteristics of sub-micrometer particles (PM1) in Guangzhou, China. Atmos. Res. 118, 222–231.

Watson, J., 2002. Visibility: science and regulation. J. Air Waste Manage. Assoc. 52, 628–713.
Xiao, R., Takegawa, N., Kondo, Y., Miyazaki, Y., Miyakawa, T., Hu, M., Shao, M., Zeng, L.M., Hofzumahaus, A., Holland, F., Lu, K., Sugimoto, N., Zhao, Y., Zhang, Y.H., 2009. Formation of submicron sulfate and organic aerosols in the outflow from the urban region of the Pearl River Delta in China. Atmos. Environ. 43, 3754–3763.
Yang, F., Chen, H., Du, J.F., Yang, X., Gao, S., Chen, J.M., Geng, F.H., 2012. Evolution of the mixing state of fine aerosols during haze events in Shanghai. Atmos. Res. 104, 193–201.
Yu, H., Wu, C., Wu, D., Yu, J.Z., 2010. Size distributions of elemental carbon and its contribution to light extinction in urban and rural locations in the pearl river delta region, China. Atmos. Chem. Phys. 10, 5107–5119.
Zauscher, M.D., Wang, Y., Moore, M.J.K., Gaston, C.J., Prather, K.A., 2013. Air quality impact and physicochemical aging of biomass burning aerosols during the 2007 San Diego wildfires. Environ. Sci. Technol. 47, 7633–7643.
Zelenyuk, A., Imre, D., Han, J.H., Oatis, S., 2008. Simultaneous measurements of individual ambient particle size, composition, effective density, and hygroscopicity. Anal. Chem. 80, 1401–1407.
Zhang, Q., Meng, J., Quan, J., Gao, Y., Zhao, D., Chen, P., He, H., 2012. Impact of aerosol composition on cloud condensation nuclei activity. Atmos. Chem. Phys. 12, 3783–3790.
Zhang, G.H., Bi, X.H., Li, L., Chan, L.Y., Li, M., Wang, X.M., Sheng, G.Y., Fu, J.M., Zhou, Z., 2013. Mixing state of individual submicron carbon-containing particles during spring and fall seasons in urban Guangzhou, China: a case study. Atmos. Chem. Phys. 13, 4723–4735.
Zhao, Y.L., Gao, Y., 2008. Acidic species and chloride depletion in coarse aerosol particles in the US east coast. Sci. Total Environ. 407, 541–547.
Zhao, M.J., Zhang, Y., Ma, W.C., Fu, Q.Y., Yang, X., Li, C.L., Zhou, B., Yu, Q., Chen, L.M., 2013. Characteristics and ship traffic source identification of air pollutants in China's largest port. Atmos. Environ. 64, 277–286.